Make research imaging workflows accessible, traceable, and secure with Athena Software for Core Imaging Facilities.

Thermo Scientific™ Athena Software is a premium imaging data management platform designed for core imaging facilities that support materials science research.

Athena Software ensures traceability of images, metadata, and experimental workflows through an intuitive and collaborative web interface.

Find out more at **thermofisher.com/athena**

ThermoFisher
SCIENTIFIC

ADVANCED FUNCTIONAL MATERIALS
www.afm-journal.de

Check for updates

Aluminum Oxide at the Monolayer Limit via Oxidant-Free Plasma-Assisted Atomic Layer Deposition on GaN

Alex Henning, Johannes D. Bartl, Andreas Zeidler, Simon Qian, Oliver Bienek, Chang-Ming Jiang, Claudia Paulus, Bernhard Rieger, Martin Stutzmann, and Ian D. Sharp**

Atomic layer deposition (ALD) is an essential tool in semiconductor device fabrication that allows the growth of ultrathin and conformal films to precisely form heterostructures and tune interface properties. The self-limiting nature of the chemical reactions during ALD provides excellent control over the layer thickness. However, in contrast to idealized growth models, it is challenging to create continuous monolayers by ALD because surface inhomogeneities and precursor steric interactions result in island growth. Thus, the ability to create closed monolayers by ALD would offer new opportunities for controlling interfacial charge and mass transport in semiconductor devices, as well as for tailoring surface chemistry. Here, encapsulation of c-plane gallium nitride (GaN) with ultimately thin (≈3 Å) aluminum oxide (AlO_x) is reported, which is enabled by the partial conversion of the GaN surface oxide into AlO_x using sequential exposure to trimethylaluminum (TMA) and hydrogen plasma. Introduction of monolayer AlO_x decreases the work function and enhances reactivity with phosphonic acids under standard conditions, which results in self-assembled monolayers with densities approaching the theoretical limit. Given the high reactivity of TMA with surface oxides, the presented approach likely can be extended to other dielectrics and III–V-based semiconductors, with relevance for applications in optoelectronics, chemical sensing, and (photo)electrocatalysis.

1. Introduction

Conformal and sub-nanometer thin dielectric layers can be grown by atomic layer deposition (ALD) at large scale and are essential for semiconductor device applications, including for gate dielectrics in field-effect transistors,[1] carrier-selective contacts in solar cells,[2] and corrosion protection layers in (photo)electrochemical cells,[3] as well as for sensing and catalysis.[4] While the properties of ALD films can be precisely controlled by substrate surface preparations, precursor chemistries, and external process parameters,[5] complex physical and chemical interactions lead to film and interface nonidealities. As a prominent example of this, ALD is often considered to proceed via layer-by-layer growth as the available surface binding sites react with a gas-phase reactant until saturation is reached, ideally resulting in the formation of one monolayer with every cycle. However, a combination of precursor steric effects, adsorption energetics, and substrate surface inhomogeneities results in incomplete surface coverage during film nucleation. As a consequence, islands form during the nucleation phase and growth of additional layers on already formed islands is unavoidable during subsequent ALD cycles. Thus, in contrast to the idealized concept of layer-by-layer growth, it is extremely challenging to create continuous films at the monolayer limit by ALD. Overcoming this gap by growing conformal monolayers offers significant opportunities for creating atomically abrupt heterostructures, as well as for tailoring the electronic properties and chemistries of surfaces to achieve controlled functionalization or passivation. Interestingly, ordered surface oxide monolayers can be formed on III–V semiconductors by chemical etching and subsequent oxide regrowth at elevated temperatures in a vacuum.[6]

In this work, we report the formation of an ultimately thin (≈3 Å), yet continuous, aluminum oxide (AlO_x) monolayer on gallium nitride (GaN) using an oxidant-free ALD process (i.e., without the use of gas-phase oxidants). To the best of our knowledge, this is the first experimental report of the formation of a closed single monolayer of AlO_x on a non-metal surface. GaN was selected owing to its established technological importance.[7] However, a major challenge of GaN and III–V semiconductor technology is to precisely engineer interface

Dr. A. Henning, J. D. Bartl, A. Zeidler, O. Bienek, Dr. C.-M. Jiang, C. Paulus, Prof. M. Stutzmann, Prof. I. D. Sharp
Walter Schottky Institute and Physics Department
Technical University of Munich
85748 Garching, Germany
E-mail: alex.henning@wsi.tum.de; sharp@wsi.tum.de
J. D. Bartl, Prof. B. Rieger
WACKER-Chair of Macromolecular Chemistry
Catalysis Research Center
Technical University of Munich
85748 Garching, Germany
S. Qian
Chair of Technical Electrochemistry
Department of Chemistry
Technical University of Munich
85748 Garching, Germany

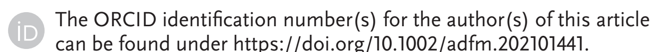
The ORCID identification number(s) for the author(s) of this article can be found under https://doi.org/10.1002/adfm.202101441.

© 2021 The Authors. Advanced Functional Materials published by Wiley-VCH GmbH. This is an open access article under the terms of the Creative Commons Attribution License, which permits use, distribution and reproduction in any medium, provided the original work is properly cited.

DOI: 10.1002/adfm.202101441

 © 2021 The Authors. Advanced Functional Materials published by Wiley-VCH GmbH

properties, which is often hampered by high concentrations of surface states. In this respect, dielectric passivation by ALD is promising as it has been demonstrated to significantly reduce interface state densities within GaN devices.[8]

A major advantage of ALD is its ability to grow defined films at low temperature, which provides versatile process compatibility and synthetic access to amorphous dielectrics that have practical advantages as passivation and interfacial layers.[9] The most widely used and industrially relevant ALD process involves trimethylaluminum (TMA) and an oxidant (typically water), sequentially introduced into a reactor chamber, to form amorphous AlO_x. TMA is an electron-deficient[10] and thus highly reactive metal–organic compound that has been applied for ALD of AlO_x at low temperatures, even below 25 °C.[11] In situ studies of the initial growth regime during ALD of AlO_x have revealed that TMA can directly react with the native oxides of III–V semiconductors, resulting in the formation of aluminum oxide via interconversion and ligand exchange reactions.[12] This high reactivity of TMA with the substrate has been previously applied to passivate the surfaces of III–V semiconductors in situ before deposition of an ALD dielectric.[12a,b] In later work, the sequential exposure of III–V surfaces to a hydrogen (H_2) plasma and TMA in an ALD process proved to be even more effective for passivation of the surface oxide layers.[13] Despite the intriguing chemical characteristics of ALD oxide interconversion reactions (also referred to as oxide clean-up reactions), neither the potential for creating ultrathin conformal oxides down to the monolayer limit nor the chemical functional characteristics of the resulting layers have been explored so far.

Understanding film nucleation is key for realizing ultimately thin coatings by ALD. Though the nucleation behavior is well established for thermal ALD of AlO_x using TMA and water,[14] less is known about film formation in oxidant-free processes involving TMA and H_2 plasma, for which the GaN surface oxide serves as the oxygen reservoir. Here, we evaluate the AlO_x growth evolution on freestanding *c*-plane GaN during cyclic exposure to TMA and atomic hydrogen by in situ monitoring of the ALD film thickness using spectroscopic ellipsometry (SE), as well as by complementary ex situ analysis using atomic force microscopy (AFM) and X-ray photoelectron spectroscopy (XPS). We find a window of self-limiting oxide growth resulting from the consumption of terminal oxygen moieties of the GaN native oxide layer during AlO_x formation. Once monolayer coverage is achieved, the surface is deactivated for subsequent chemisorption of TMA, resulting in self-limited growth with no island formation. The thickness of the closed layer, independently measured by SE, AFM, and XPS to be ≈3 Å, agrees well with the theoretically predicted thickness for a single monolayer.[15] Creation of this single AlO_x monolayer leads to a significant reduction of the work function of GaN by 0.38 eV. Furthermore, relative to the solvent-cleaned GaN surface, the monolayer AlO_x provides additional chemical functionality, which is highlighted by its high reactivity with phosphonic acids to form self-assembled organic monolayers with a coverage that approaches the theoretical limit at room temperature. Thus, the GaN/monolayer AlO_x system provides a novel platform for creating self-assembled monolayers with strong electronic coupling to the underlying semiconductor owing to the absence of an extended interlayer.

2. Results and Discussion

As a starting point for elucidating the growth of AlO_x on GaN substrates via the oxidant-free plasma-assisted ALD process, in situ spectroscopic ellipsometry was used to track film thickness dynamics during the different steps of each cycle, as well as over multiple successive cycles. We used a Cauchy dispersion model with the parameters for alumina (Section S3, Supporting Information) after having confirmed the presence of AlO_x by XPS. As shown in **Figure 1a**, which provides a plot of film thickness as a function of time, three different growth regimes can be distinguished during 100 cycles of TMA and H_2 plasma exposure. These regimes are characterized by: i) growth with an exponentially decaying rate, ii) a saturated film thickness with a growth rate of zero, and iii) slow growth with an approximately constant rate. Each of these is discussed in detail below.

In regime (i), the growth per cycle (GPC), which is defined as the measured change in layer thickness per cycle, follows an exponential decay and reaches saturation (i.e., GPC = 0 Å) after eight cycles with a thickness of 2.8 ± 0.1 Å (Figure 1b). The origin of this saturation behavior can be understood by considering the detailed growth mechanism. As shown in Figure 1b, the first few cycles exhibit the largest GPC, which suggests a substrate-enhanced growth governed by the accessible binding sites on the GaN surface.[16] This stands in contrast to the growth characteristics of traditional thermal ALD of AlO_x on GaN using TMA and H_2O, in which growth is inhibited during the initial cycles (Figure 1b,c).

XPS analysis revealed that the surface of GaN is coated with an ≈1 nm thin native oxide layer that is terminated with OH groups (Section S5, Supporting Information). The thickness of this native oxide layer was confirmed by X-ray reflectivity (XRR) (Figure S2, Supporting Information) and agrees with the literature.[17] Consistent with XPS analysis, static water contact angle measurements of these surfaces exhibit hydrophilic character, with contact angles of ≈39° and ≈34° obtained before and after the initial H_2 plasma treatment, respectively (Table S2, Supporting Information). This hydrophilicity indicates that the native gallium oxide surface is partially hydroxylated, thereby providing Ga—OH binding sites that can react with TMA through a ligand-exchange reaction, in a manner similar to TMA reacting with SiO_2.[14a] As a consequence, exposure to TMA results in the formation of AlO_x according to the following ligand exchange reaction[18]

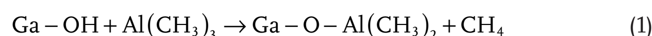

$$\mathrm{Ga-OH+Al(CH_3)_3 \rightarrow Ga-O-Al(CH_3)_2+CH_4} \quad (1)$$

Although Reaction (1) is self-limiting, the available binding sites cannot be completely consumed after one TMA half-cycle owing to steric hindrances. In particular, binding sites are shielded by the methyl groups of neighboring chemisorbed TMA molecules and may also be blocked by physisorbed TMA molecules and clusters. While weakly bound TMA molecules are swept away from the surface during argon (Ar) purging, the ligands of chemisorbed TMA molecules will remain until chemically reactive species are introduced. As indicated by the red arrows of Figure 1b, subsequent H_2 plasma exposure leads to a decrease in the adsorbate thickness, indicating that atomic hydrogen, which is used here instead of an oxidant, reduces the

© 2021 The Authors. Advanced Functional Materials published by Wiley-VCH GmbH

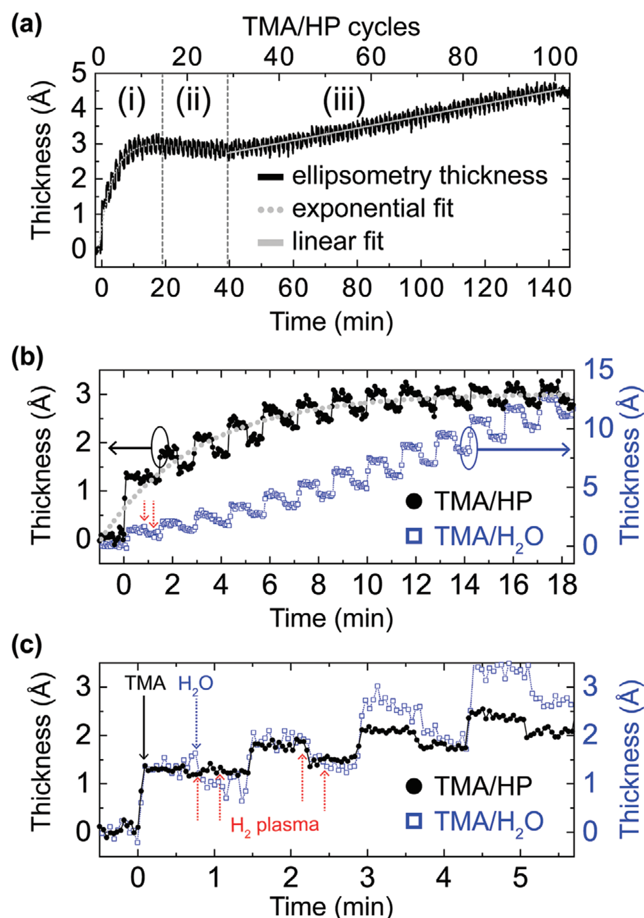

Figure 1. a) Plot of the ALD layer thickness as a function of time, determined via in situ spectroscopic ellipsometry. Three different growth regimes (i–iii) can be distinguished. b) Zoom-in of the thickness–time plot showing growth regime (i), in which the growth per cycle exponentially decreases before saturation at ≈3 Å. For comparison, the thickness–time plot of a thermal ALD AlO_x process with H_2O is shown (blue, thickness scale given by right axis). c) Zoom-in of the thickness–time plot showing the first four cycles. The black, blue, and red arrows indicate TMA injections, H_2O injections, and plasma times, respectively, for the first two cycles. The reactor temperature was maintained at 280 °C, and freestanding *c*-plane GaN substrates were used for both recipes.

adsorbed TMA via the formation of methane. Consequently, Ga—OH binding sites that were blocked by methyl ligands after the first TMA half-cycle become accessible for subsequent reactions with TMA. This simple mechanistic model predicts an exponential decay of available binding sites[19] and explains the observed exponential decrease of the individual cycle growth rate over successive cycles.

A critical aspect of this oxidant-free AlO_x ALD mechanism is that the surface is chemically deactivated as the Ga—OH sites are consumed, as indicated by the observed decrease of the GPC, which reaches zero after eight TMA/hydrogen plasma cycles. As exposure to hydrogen plasma reduces the methyl ligands of chemisorbed TMA to methane, an O—Al* terminal surface, which may include partial coverage by O—Al—CH_3 sites, is established. This surface composition inhibits further chemisorption of TMA and, thus, the growth of subsequent layers, thereby giving rise to regime (ii), during which the thickness remains nearly constant (Figure 1a,b). In addition, the in situ SE measurements reveal that the AlO_x film is not chemically reduced upon exposure to several cycles of low power H_2 plasma. Here, we note that the AlO_x-coated GaN exhibits a water contact angle of ≈8°, which indicates a strongly hydrophilic surface (Table S2, Supporting Information) that is consistent with an Al—OH surface termination. However, these measurements require exposure to ambient atmosphere, which is expected to rapidly oxidize the —Al* termination, thereby introducing hydrophilic oxygen groups on the surface.

The proposed growth mechanism resembles a Frank–van der Merwe type of growth, in which TMA reacts preferentially with substrate surface sites, resulting in complete surface coverage. However, in contrast to conventional growth modes, deposition of subsequent layers is suppressed owing to chemical deactivation of the surface. Importantly, this chemical inactivity reduces the likelihood of island formation[14b] and provides the intriguing opportunity for ideally self-saturating growth of AlO_x down to the single monolayer limit. To explore this possibility, we consider the saturated AlO_x film thickness and compare it to the predicted monolayer thickness, which can be estimated according to Equation (2)

$$h_{\mathrm{ml}} = \left(\frac{M}{\rho N_{\mathrm{A}}}\right)^{1/3} \tag{2}$$

where M, ρ, and N_A are the molar mass, density, and Avogadro constant, respectively. For an ultrathin layer of this type, it is difficult to determine the density. However, reasonable values can be obtained from prior reports of ALD alumina, which yield values in the range of 3.2–3.5 g cm^{-3} at similar substrate temperatures.[20] At the level of a monolayer, half the volume of the α-Al_2O_3 unit cell (i.e., a nominal composition of $AlO_{1.5}$) is assumed, which yields an approximate thickness, h_{ml}, in the range of 2.89–2.98 Å. Thus, the film thickness in the saturation regime (ii) of 2.8 ± 0.1 Å, determined experimentally via in situ spectroscopic ellipsometry, is in excellent agreement with the predicted thickness of a single monolayer of alumina. This agreement is fully consistent with the proposed film formation mechanism and offers fascinating possibilities for the establishment of 2D dielectric interlayers, as discussed below.

Although no growth is observed for several subsequent TMA/H_2 plasma cycles, a third growth regime, indicated as the region (iii) in Figure 1a, emerges after 20 cycles. This regime is characterized by a constant, but slow, growth rate of 0.03 Å $cycle^{-1}$. According to the model discussed above, no such growth would be expected. However, in situ SE measurements suggest that repetitive exposure to H_2 plasma and TMA pulses leads to accumulation of material on the surface. Although the origin of this growth regime is not conclusively known, it is apparent that TMA precursor adsorption on the surface must occur, but with very low coverages, suggesting a potential role of defects as binding sites. Chemical interactions of TMA and such nonidealities may yield dissociative chemisorption,[21] and the cumulative effect of repetitive H_2 plasma exposure would then result in a complete reduction to elemental Al as no oxygen from the underlying oxide is accessible. To confirm the feasibility of

© 2021 The Authors. Advanced Functional Materials published by Wiley-VCH GmbH

metallic Al growth, we prepared a sample using 200 cycles of TMA/H_2 plasma at a higher plasma power (300 W). The larger growth rate (GPC ≈ 0.15 Å) resulted in Al films that are sufficiently thick to not completely oxidize in air. XPS analysis of the resulting surfaces revealed an Al 2p component at a lower binding energy (≈72.9 eV), indicative of metallic Al, alongside the higher binding energy feature associated with Al—O binding (≈75.6 eV) (Figure S10, Supporting Information). This result, which is consistent with the prior report of metallic Al ALD using TMA/H_2 plasma cycles,[22] lends additional credence to the proposed description of linear growth in regime (iii).

We now return to a detailed analysis of the characteristics of the ultrathin AlO_x layer formed prior to the onset of regime (iii), as well as the properties of its interface with GaN. To assess ALD film conformality and surface roughness, both solvent-cleaned GaN and GaN/AlO_x were characterized by AFM. The AFM height images before and after 20 cycles of TMA and H_2 plasma exposure showed a nearly identical root mean square (rms) roughness of 237 ± 6 pm and 228 ± 3 pm, respectively, indicating the formation of a uniform and continuous ALD film conforming to the topography of the GaN surface (**Figure 2a**,b). The normalized height distributions of solvent-cleaned and TMA/H_2 plasma-treated GaN follow symmetric Gaussian lineshapes (skewness = ±0.05, kurtosis = 2.95) typical of homogenous surfaces with randomly distributed height variations. No indications of pinholes or island growth were observed, which is consistent with the proposed self-limiting growth mechanism. While the results presented in Figure 2 were obtained from freestanding GaN, similar results were obtained for the case of epitaxial GaN thin films on sapphire substrates (Figure S14a,b, Supporting Information). For reference, the AFM topography of a film with the same SE-measured thickness of ≈0.3 nm formed using a thermal ALD process with TMA and H_2O reveals the presence of islands, resulting in a larger roughness (Figure S14c, Supporting Information). This comparison highlights the unique ability of the H_2 plasma/TMA process for forming a closed alumina monolayer.

Following characterization of the topography, a diamond-like carbon (DLC) tip was used to abrade the AlO_x monolayer in contact mode, as previously demonstrated with thicker ALD AlO_x films on Si substrates.[23] The subsequently acquired AFM phase and height images suggest the presence of a continuous AlO_x monolayer with a thickness of 3 ± 1 Å (Figure S15, Supporting Information), consistent with the thickness derived from SE measurements.

XPS was performed to determine the chemical changes to the surface arising from exposure of GaN to 20 cycles of TMA and H_2 plasma. **Figure 3a** shows the Ga 3d core level region of the solvent-cleaned GaN surface, within which Ga—N, Ga—O, and Ga—Ga, as well as N 2s components can be discriminated. Spectral fitting was achieved by constraining the spin–orbit splitting to be 0.43 eV[24] with an area ratio of 3:2 and equal full width at half maximum (FWHM) for both components of the 3d doublets. For both the solvent-cleaned and TMA/H_2 plasma-exposed sample, the magnitude of the shift of the Ga—O components relative to the main Ga—N photoemission is consistent with prior studies[25] and indicates the presence of a native oxide comprising primarily Ga_2O_3. Ga 3d photoelectrons emitted from Ga—O—Al environment are expected to shift towards lower BEs, i.e., closer to the Ga—N main peak because of the relatively lower electronegativity of aluminum. Indeed, XPS analysis indicates that the Ga—O/Ga—N ratio decreased after the TMA/H_2 plasma process (Figure 3a, inset). This finding suggests an AlO_x film growth mechanism that includes the formation of Ga—O—Al bonds,[26] which is in agreement with the proposed Reaction (1) based on the real-time SE data, as well as previous reports of TMA reactivity on GaN[25,27] and AlGaN[28] during traditional thermal ALD using H_2O as an oxidant.

The Al 2p core level spectrum is well described by a single component with a binding energy of 75.40 eV, which can be assigned to an Al—O environment (Figure 3b). Comparison of the 1.71 eV FWHM to the instrumental resolution of ≈0.30 eV (Figure S6, Supporting Information) indicates significant inhomogeneous broadening that is typical of amorphous materials. By comparison, the Al 2p peak of a 25 nm thick AlO_x reference film grown by thermal ALD (250 cycles of TMA/H_2O, 280 °C) on GaN has an FWHM of 1.43 eV (Figure S11, Supporting Information), in agreement with prior literature reports.[29] The O 1s spectra of solvent-cleaned and AlO_x-coated GaN substrates reveal two chemical components attributed to hydroxyl groups and metal-oxide bonds (Figure S8, Supporting Information).

It is expected that the hydroxylated monolayer AlO_x coating should enhance surface basicity (acid-base reactivity), thereby providing the opportunity to introduce new chemical

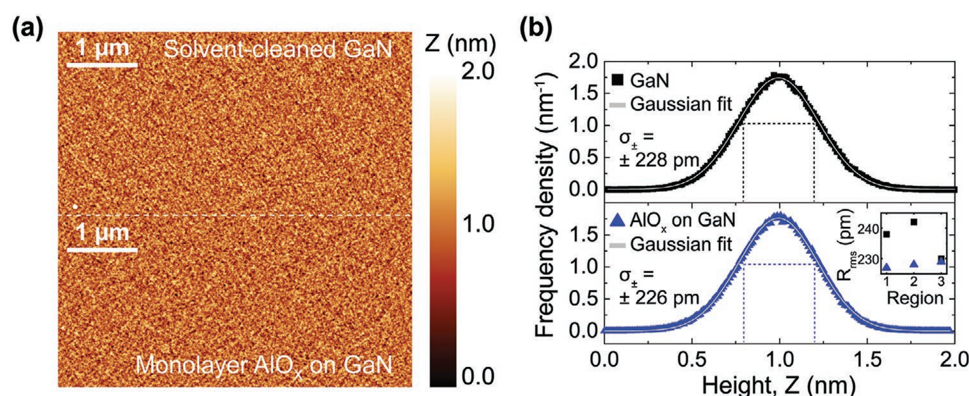

Figure 2. a) AFM topographs of solvent-cleaned (upper image) and monolayer AlO_x-coated GaN (lower image) following 20 ALD cycles of H_2 plasma and TMA. b) Frequency densities extracted from the AFM height images follow a Gaussian distribution with nearly identical parameters.

© 2021 The Authors. Advanced Functional Materials published by Wiley-VCH GmbH

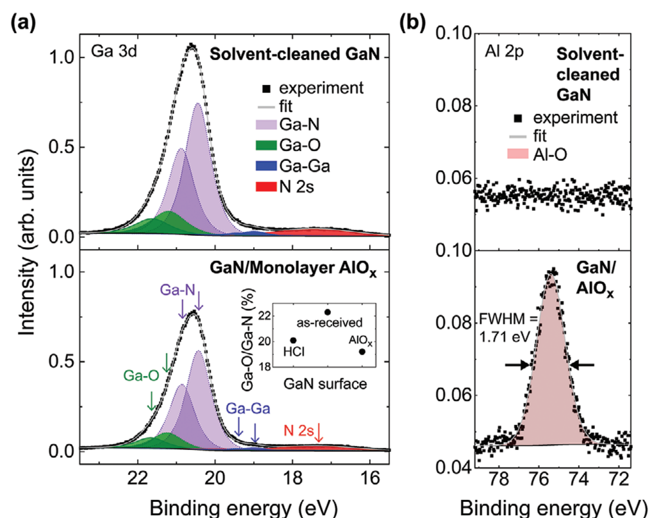

Figure 3. X-ray photoelectron spectra of a) Ga 3d and b) Al 2p core levels of solvent-cleaned GaN (top row) and monolayer AlO_x-coated GaN (bottom row). The inset in (a) shows the average gallium oxide concentrations for solvent-cleaned, HCl-etched, and monolayer AlO_x-coated GaN surfaces.

functionality to the surface. To test this hypothesis, we investigated the reactivity of the ALD-modified GaN surface with phosphonic acids (PAs) under standard conditions. The PA head group binding sites, namely, the acidic hydroxyls and the phosphoryl group, can react with the hydroxyl groups of the substrate via an acid-base heterocondensation.[30] While this reaction requires thermal activation for acidic and weakly basic (Lewis acidity) hydroxylated surfaces, such as the native oxides of Ga[31] and Si,[32] it can occur under standard conditions for basic hydroxylated substrates, such as aluminum oxide.[33] To test the reactivity of the ALD-modified surface, we performed an organophosphonic acid functionalization reaction with 11-hydroxyundecylphosphonic acid (PA-C11-OH) via a modified immersion technique at room temperature and atmospheric pressure (Section S7, Supporting Information). While a large variety of different PAs with different dipole moments and functional groups can be anchored using this approach, PA-C11-OH was selected because of its functional end group (OH), which enables additional molecular architectural steps.

The AFM topography (**Figure 4a**,b) demonstrates a uniform and smooth organic SAM with an rms roughness of 274 ± 9 pm, thereby providing further evidence of a continuous AlO_x coating. An average organic SAM thickness of ≈5.8 ± 0.4 Å was determined from the step heights after removal of the organic layer in contact mode AFM (Figure 4a,b). Considering the length of PA-C11-OH and the measured SAM thickness, a molecular tilt angle, θ, of 70.5 ± 2.8° with respect to the surface normal was determined. This value is relatively large compared to prior literature reports of PA-C11-OH SAMs. For example, (100) Si yields tilt angles of ≈45°.[34] However, the tilt angle and thus the SAM thickness are related to the PA binding configuration, which is known to be affected by the deposition method, PA structure, and surface coverage.[35] In particular, the PA can interact with the underlying AlO_x layer via P—O—Al bonding in mono-, bi-, or tridentate modes, depending on the number

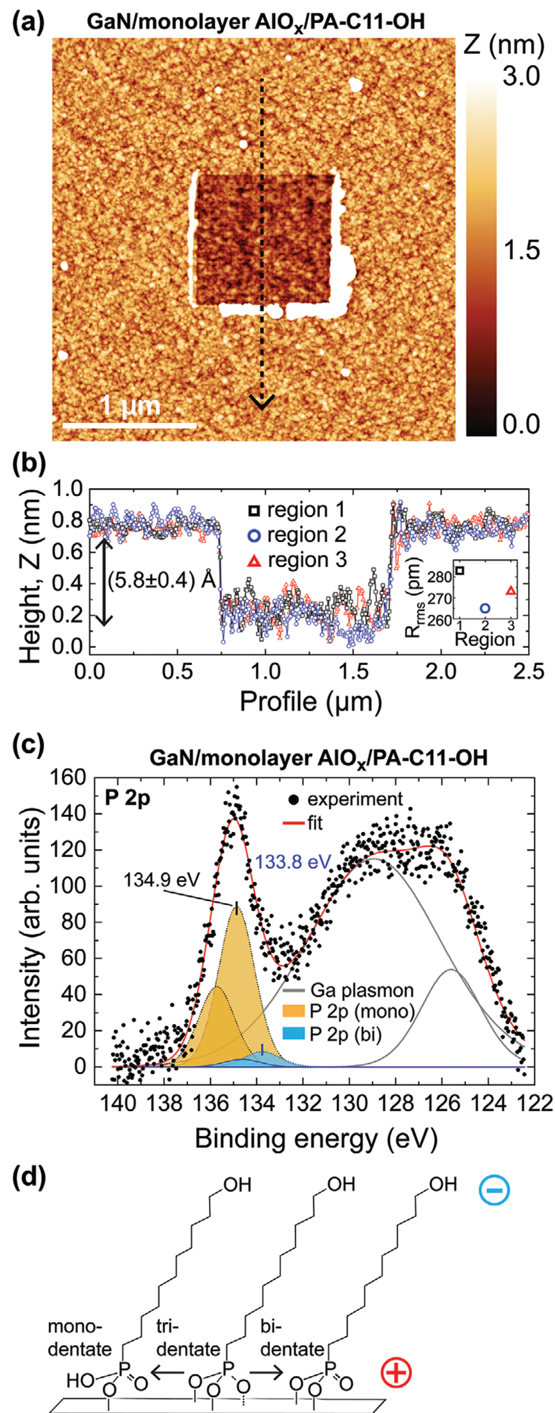

Figure 4. a) AFM topography of monolayer AlO_x-coated GaN functionalized with PA-C11-OH showing a center region where the organic layer was removed by contact mode AFM. b) Height profiles collected in three different regions, each located a few mm apart from one another, indicating the homogeneity of the SAM layer and allowing determination of the thickness. c) P 2p photoelectron spectrum and corresponding fit of the GaN/monolayer AlO_x/PA-C11-OH sample. P 2p spin–orbit splitting and Ga plasmons are considered in the fit, which suggests a mostly monodentate binding motif (P 2p (mono)) of the PA head group to the monolayer AlO_x. d) Schematic representation of three possible binding configurations of PA-C11-OH on a hydroxylated surface.

© 2021 The Authors. Advanced Functional Materials published by Wiley-VCH GmbH

of PA functional groups that are involved, as indicated in Figure 4d.[30] Previously, bidentate bonding was reported to be dominant for GaN following functionalization at elevated temperature,[36] while a range of different binding motifs has been reported for aluminum oxide surfaces.[35]

To probe the binding motif and quantify the molecular coverage, XPS measurements were performed on functionalized surfaces. Figure 4c shows a typical XPS spectrum of the P 2p core level region, which also includes the Ga 3p plasmon, for a GaN/monolayer AlO_x/PA-C11-OH sample. Despite a theoretical spin-orbit splitting of 0.9 eV,[37] the main P 2p peak at 135 eV is broad (FWHM = 1.79 eV) and approximately symmetric, which is consistent with a mixture of binding modes.[37,38] The optimum fit of the P 2p spectrum (Figure 4c, red line) suggests a combination of two binding configurations, of which the monodentate binding motif is dominant (88 ± 3%).

Prior reports attributed the evolution from higher to lower denticities to an increasing SAM surface coverage.[38,39] Our results are consistent with this finding since we observe a relatively large phosphorus atom density of $(4.5 \pm 0.3) \times 10^{14}$ cm^{-2}, corresponding to a PA surface coverage, n, of 4.5 ± 0.3 nm^{-2}, as calculated from the XPS data (Figure 4c) according to the formalism introduced by Kim et al.[31] (Section S7, Supporting Information). This high SAM surface coverage (4.5 ± 0.3 nm^{-2}) on GaN/monolayer AlO_x approaches the theoretical limits predicted for aluminum oxide surfaces (4.3–4.7 nm^{-2})[40] by density functional theory (DFT) and estimated from the molar volume of phosphorus acid (4.25 nm^{-2}),[41] and it is two times higher than reported for alkyl-PAs grafted on *c*-plane- Ga-polar GaN (2.3 nm^{-2}).[31] These high coverages are consistent with the formation of a continuous AlO_x coating, onto which the PAs molecules assume a predominantly monodentate binding motif in a high-density SAM.

Having established the surface chemistry of the GaN/monolayer AlO_x system, we next focus on the effect of the monolayer AlO_x coating on the surface energetics, which can influence electrical transport, surface chemical reactions, and dipole interactions. To quantify how the deposition of monolayer AlO_x and SAM functionalization affect the work function, Φ, and surface band bending of GaN, we performed contact potential difference (CPD) and surface photovoltage (SPV) measurements in a vacuum (**Figure 5a**). After deposition of monolayer AlO_x on GaN, CPD measurements indicate that the work function decreases by 0.38 eV compared to solvent-cleaned GaN. Concurrently, SPV measurements reveal an upward band bending of 0.49 eV, which is the same for both solvent-cleaned GaN and monolayer AlO_x/GaN. This is consistent with XPS measurements, which are sensitive to changes of band bending but not work function: here, XPS revealed that the VB edge positions (Figure S12, Supporting Information) and core level BEs (Table S4, Supporting Information) were not affected by the presence of the AlO_x monolayer to within the measurement error. Thus, changes to the interfacial energetics can be explained in terms of a change of the surface dipole associated with monolayer AlO_x deposition (Figure 5b). The polarity of this dipole, for which the positive endpoints are outward, is consistent with the smaller electronegativity of Al (1.7[42]) relative to Ga (2.4[42]). In addition, polarization-induced negative bound charges of the Ga-polar GaN may facilitate interface dipole formation as these surface charges are compensated by the native GaO_x layer,[43] rendering the GaO_x at the GaN/GaO_x interface more positive compared to the GaO_x surface. The microscopic dipole that forms at the interface between the native GaO_x film and the sub-stoichiometric monolayer AlO_x results in an abrupt change of the vacuum level that reduces the effective work function (Figure 5b). The bound charge density, σ, at the monolayer AlO_x/GaO_x interface can be estimated using Gauss' theorem, $\sigma = \frac{|\Delta V_{AlOx}| \varepsilon_{eff} \varepsilon_0}{d e_0}$, where $|\Delta V_{AlOx}|$ is the magnitude of the measured CPD change after monolayer AlO_x deposition, $\varepsilon_{eff} = \frac{2\varepsilon_{AlOx}\varepsilon_{GaOx}}{\varepsilon_{AlOx} + \varepsilon_{GaOx}}$ is the effective dielectric constant, d, is the separation between positive and negative point charges of the dipole layer, and e_0 is the elementary charge. Assuming $d = 3$ Å as the average distance between Ga and Al atoms at the Ga−O−Al interface, $\varepsilon_{AlOx} \approx 4$ for ultrathin ALD AlO_x[19] and $\varepsilon_{GaOx} \approx 9$ for amorphous GaO_x[44] yields $\sigma \approx 3.5 \times 10^{13}$ cm^{-2}, which is in the range of polarization-induced charge densities of polar GaN. We note that in addition to the interface dipole, fixed charges of both polarities have been measured for thicker AlO_x films by resonant XPS,[45] predicted by DFT calculations,[46] and quantified by capacitance–voltage measurements, respectively.[47,48]

CPD measurements were also performed to determine how the PA-C11-OH SAM affects the surface energetics relative to the solvent-cleaned GaN and GaN/AlO_x surfaces, as shown in Figure 5a. The measured increase in the CPD after GaN/monolayer AlO_x surface functionalization with a PA-C11-OH organic monolayer is consistent with the presence of a surface dipole that arises from the permanent OH surface termination introduced by the SAM (Figure 5c). The surface dipole introduced by the AlO_x monolayer is in the opposite direction to the SAM dipole and therefore may account for the large tilt angle of the organic layer. The out-of-plane component of the dipole moment, μ_z, of an adsorbed monolayer can be calculated using the Helmholtz relationship, $\mu_z = \frac{\Delta V_{PA} \varepsilon_{PA} \varepsilon_0}{n \cos\theta}$,[49] where ε_{PA} is the relative dielectric constant, ε_0 is the vacuum permittivity, and n is the areal density of adsorbed molecules (dipoles). Inserting the surface coverage of 4.5×10^{14} cm^{-2} derived from XPS analysis, the measured change of the CPD, ΔV_{PA}, of 0.18 V, and the reported alkyl SAM permittivity, ε_{PA}, of 3,[50] yields a surface dipole of +0.32 D. By correcting for the tilt angle, $\theta \approx 71°$ deduced from the measured SAM thickness (Figure 5b), the surface dipole of a vertically aligned PA-C11-OH monolayer would equal +0.95 D. While this value is lower than the reported free molecule dipole moment (+1.46 D) predicted by density functional theory,[51] it has been established that depolarization within SAMs leads to a deviation between the free molecular dipole and the bound molecular dipole, of which the latter was found to correlate with observed changes in the work function.[52] Here, we find that surface energetics of the GaN are significantly modified by the introduction of a single monolayer of AlO_x and can be additionally tuned by the introduction of a molecular monolayer, whose assembly is enabled by the chemical functionality of the ALD oxide.

© 2021 The Authors. Advanced Functional Materials published by Wiley-VCH GmbH

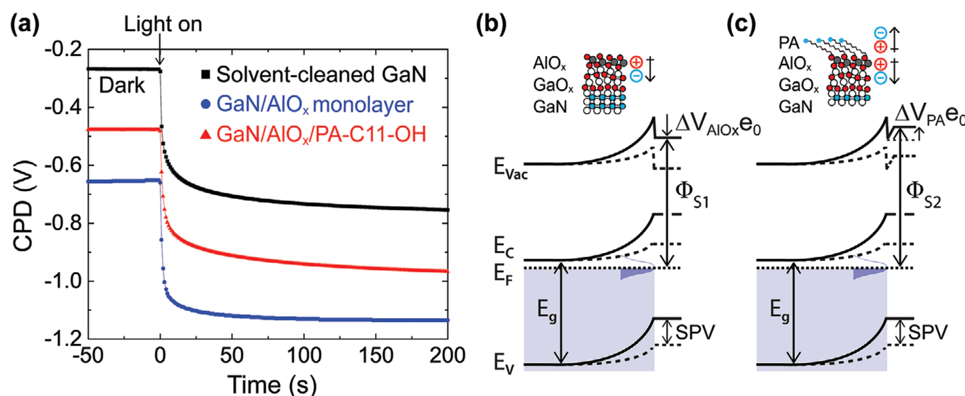

Figure 5. a) CPD evolution for the three sample systems: solvent-cleaned GaN (black squares), monolayer AlO_x-coated GaN (blue circles), and GaN/monolayer AlO_x/PA-C11-OH (red triangles). The SPV is measured with above-bandgap illumination (340 nm wavelength). b,c) Schematic band diagrams and illustrations of the GaN/GaO_x/monolayer AlO_x and GaN/GaO_x/monolayer AlO_x/PA-C11-OH samples, respectively, in which the + and – indicate the dipole orientations in the different layers.

3. Conclusion

The presented oxidant-free ALD process (i.e., without the use of gas-phase oxidants) allows for the fabrication of conformal oxide coatings down to the single monolayer limit. This was demonstrated via the deposition of a monolayer AlO_x film on GaN, which was accomplished by oxidant-free ALD with TMA and H_2 plasma. The TMA/H_2 plasma growth process self-terminates after complete surface coverage with AlO_x because the TMA preferentially reacts with the surface sites on the gallium oxide, but not the formed AlO_x layer, thereby preventing vertical (three-dimensional) growth. The average thickness of the sub-nanometer thin AlO_x coating on the GaN surfaces was determined with statistical confidence by SE and XPS and is consistent with the predicted monolayer AlO_x thickness. The ultrathin AlO_x coating increases surface hydrophilicity and basicity, facilitating the formation of a stable SAM under standard conditions with a coverage approaching the theoretical limit, thereby allowing additional tuning of interfacial energetics and the controlled introduction of chemical moieties at the terminal surface.

This work demonstrates, to the best of our knowledge, the first experimental realization of monolayer AlO_x on a non-metal surface. As a perspective, it should be feasible to extend the presented monolayer AlO_x scheme based on self-terminating reaction with a surface oxide layer to the broader range of III–V semiconductors for the formation of different monolayer coatings derived from ALD precursors possessing strong reduction potentials (e.g., tetrakisdimethylamido-hafnium). In this regard, substrates with crystalline surface oxides (e.g., demonstrated for GaN[53] and for AlGaN[54]) potentially provide a route to the creation of highly ordered alumina monolayers, opening intriguing opportunities for further studies of engineered interfaces. Importantly, this approach overcomes a major non-ideality of traditional ALD by eliminating island formation during the growth. Thus, it offers a powerful approach for realizing precise heterostructures by fulfilling the rigorous definition of atomic layer deposition. The resulting control of surface chemistry and energetics at the single monolayer level provides functional control of surfaces tailored for use in chemical sensing, (photo)catalysis, high electron mobility transistors, and advanced optoelectronic devices.

4. Experimental Section

GaN Substrates: Freestanding and unintentionally silicon (Si) doped (resistivity < 0.5 Ω cm; donor density $\leq 1 \times 10^{17}$ cm^{-3}) *c*-plane Ga-polar GaN substrates (10 × 10.5 mm^2), grown by hydride vapor phase epitaxy (HVPE) by the Nanowin Science and Technology company (Suzhou, China) were used for the ALD nucleation study, as well as for surface functionalization and chemical analysis by XPS. The GaN substrates have a nominal dislocation density below 1×10^6 cm^{-2} and were chemomechanically polished (epi-ready) by the manufacturer. Prior to characterization and ALD processing, the GaN substrates were sonicated (37 kHz, 120 W) successively in acetone, isopropanol, and deionized water for 10 min, respectively, and blow-dried by nitrogen. X-ray diffraction (XRD) was performed with a Rigaku SmartLab diffractometer equipped with a Cu anode and a 2 × Ge(220) monochromator. XRD analysis confirmed that the substrate surface is parallel to the *c*-plane of GaN (Figure S1, Supporting Information). Diffraction peaks from the (20-24) plane are separated by 60°, consistent with the six-fold symmetry of the hexagonal structure of wurtzite GaN. The FWHM of the X-ray rocking curve for the (0002) plane is 87 arcsec, verifying the high crystal quality of the GaN. Templated *c*-plane GaN layers on sapphire were used for static water contact angle measurements (Section S4, Supporting Information) and AFM characterization (Figure S14, Supporting Information). Single side polished 20 µm thick *c*-plane, Ga-polar GaN templates (Si-doped, carrier concentration > 1×10^{17}, dislocation density < 5×10^8 cm^{-2}) grown by HVPE on 430 ± 25 µm thick sapphire substrates were obtained from MSE supplies LLC (Arizona, USA). The individual GaN wafers were cut into 10 × 10 mm^2 pieces.

Atomic Layer Deposition: GaN substrates were coated with AlO_x in a hot-wall plasma-enhanced atomic layer deposition (PE-ALD) reactor (Fiji G2, Veeco CNT) in continuous flow mode. An in situ H_2 plasma pretreatment (2 cycles, 3 s, 100 W, 0.02 Torr) at 280 °C was performed to remove the ≈5 Å thin adsorbate layer of air-exposed GaN (Figure S4, Supporting Information) prior to deposition of alumina. While this relatively short remote H_2 pretreatment was mainly done to remove water and carbon impurities, and thus to establish the precondition for homogenous ALD film nucleation,[26] we note that prolonged (1–5 min) forming gas (H_2/N_2 mixture) and N_2 plasma treatments have been shown to remove the surface oxide layer[55] and reduce the surface and interface state density of III–V semiconductors.[56] Depending on the exposure conditions (pressure, temperature, radical concentration), hydrogen plasma can have detrimental effects on the structural and electronic properties of GaN and AlGaN,[56a] and it may also improve the surface quality by passivating dangling bonds on GaN.[57] In the present work, SE indicates no significant change to the thickness of the native oxide layer during brief remote H_2 plasma exposure. AlO_x films

© 2021 The Authors. Advanced Functional Materials published by Wiley-VCH GmbH

were grown using TMA (electronic grade, 99.999%, STREM Chemicals) as the precursor and Ar (99.9999%, Linde) as the carrier gas during the first half-cycle at ≈0.09 Torr while the turbo pump was isolated. The pressure–time plot (Figure S5, Supporting Information) illustrates the ALD AlO_x growth process, which has previously been implemented with similar parameters for the in situ preparation and passivation of III–V semiconductor surfaces before deposition of dielectrics.[13a,58] The precursor and plasma doses were set such that the reactions with the GaN surface were self-limiting, which was determined by in situ SE monitoring of the adsorbate thickness during plasma and TMA dose tests. The reactor wall and chuck temperatures were controlled to 280 °C, i.e., below the TMA decomposition temperature (≥300 °C). During the second half-cycle, H_2 (99.9999%, Linde) was supplied as the carrier and plasma gas at a base pressure of 0.02 Torr, which was achieved with a turbo pump. H_2 plasma was generated in a sapphire tube with an inductively coupled plasma source, where a radio frequency (RF) bias at 13.64 MHz and 100 W was applied to a copper coil wrapped around the sapphire tube. Each cycle of ALD AlO_x followed the sequence: 0.08 s TMA dose, 30 s Ar purge, 10 s H_2 purge, 2 s H_2 plasma, 10 s Ar purge, 10 s H_2 purge, 2 s H_2 plasma, 10 s Ar purge.

Preparation of Self-Assembled Monolayers of Phosphonic Acids (SAMPs): SAMPs of 11-hydroxyundecylphosphonic acid (≥99% (GC); referred to as PA-C11-OH) (SiKÉMIA, Montpellier, France) were prepared via a modified immersion technique, which is described in detail in Section S7 (Supporting Information).

Spectroscopic Ellipsometry: Changes in the GaN surface oxide layer thickness were monitored in real time using an in situ ellipsometer (J.A. Woollam, M-2000) with a sampling time of ≈3 s during ALD. The light of a Xenon lamp (Hamamatsu, L2174-01) was focused to a spot area of ≈5×8 mm^2 onto the sample surface. The incoming and reflected light passed through fused silica quartz windows (Lesker, VPZL-275DU) arranged in a fixed angle (67°) geometry. The dwell (purge) times after each precursor and plasma step were programmed to be at least three times the SE integration time. A general oscillator model was used to model changes of the polarization in the wavelength range around the GaN bandgap, i.e., between 210 and 400 nm (Figure S3, Supporting Information).

X-Ray Photoelectron Spectroscopy: XPS spectra were acquired in the hybrid lense mode at pass energy of 10 eV and a take-off angle of 0° with a Kratos Axis Supra setup equipped with a monochromatic Al Kα X-ray source (photon energy = 1486.7 eV) operated with an emission current of 15 mA. The beam area was set to ≈2×1 mm^2 using the slot collimation mode. The binding energy of the hemispherical analyzer was calibrated with in situ sputter-cleaned silver, gold, and copper standard samples. Thereby, the kinetic energies of the Ag 3d (1118.51 eV), Au 4f (1402.73 eV), and Cu 2p (554.07 eV) core levels were referenced with an accuracy of 25 meV to the known peak values. Charge neutralization was not required as no binding energy shifts indicative of (differential) charging were observed for the freestanding not intentionally doped *n*-type GaN samples. The instrumental broadening (0.30 eV) was determined by fitting of the measured Ag 3d core level spectrum of a silver calibration sample with a Voigt function (Figure S6, Supporting Information). To facilitate the quantitative analysis of compositions and film thicknesses, the surface adsorbate layer (water and adventitious carbon) of the ambient-exposed GaN samples was selectively removed by mild sputtering with Ar_{1000}^{+}-ion clusters (10 keV, 60 s, 37° incidence angle) generated with a gas cluster ion source (GCIS). Comparison of GaN core level spectra before and after sputter cleaning demonstrates the attenuation effect of the carbon overlayer on GaN core level emission intensities (Figure S7, Supporting Information). The mild in situ Ar-ion cluster sputter procedure was optimized to selectively remove the surface adsorbates without altering the chemical bonds in the GaN, as confirmed by the identical Ga 2p and Ga 3d core level peak shapes before and after sputtering.

Atomic Force Microscopy: AFM measurements were carried out with a Multimode V microscope (Bruker) in ambient using NSG30 AFM probes (TipsNano) with a nominal tip radius of 8 nm, typical resonance frequency of 320 kHz and force constant of 40 N m^{-1}. Height images (5×5 µm^2 and 3×3 µm^2) were acquired at a scan rate of 0.5 Hz with 512-point sampling. A diamond-like carbon probe (Tap190DLC, BudgetSensors) with a nominal radius of 15 nm was used to locally remove the AlO_x monolayer and self-assembled monolayers in contact mode with tip-sample forces of 3.25 and 0.65 µN, respectively. The tip-sample force, F_{ts}, in hard contact with the surface, was calculated using Hooke's law, $F_{ts} = ks$, where the measured deflection, s, was determined from a force–distance curve and the spring constant, k, was obtained from a thermal tune. Height images (5×5 and 3×3 µm^2) were acquired at a scan rate of 0.5 Hz with 512-point sampling.

Kelvin Probe (KP) and SPV Characterization: SPV measurements were carried out in vacuum (≤1×10^{-5} bar) at room temperature using a custom-built setup equipped with a commercial Kelvin probe and controller (Kelvin Probe S and Kelvin Control 07, Besocke DeltaPhi) and a focused light-emitting diode with a wavelength of 340 nm (M340L4, Thorlabs) and intensity of ≈35 mW cm^{-2}. A piezoelectrically driven gold grid with a diameter of 3 mm and a work function of ≈4.9 eV was used as the reference electrode. The time resolution of the CPD measurements was 1.0 s.

Supporting Information

Supporting Information is available from the Wiley Online Library or from the author.

Acknowledgements

This work was supported by the Deutsche Forschungsgemeinschaft (DFG, German Research Foundation) under Germany's Excellence Strategy (EXC 2089/1 – 390776260) and by the DFG through the TUM International Graduate School of Science and Engineering (IGSSE). A.H. acknowledges funding from the European Union's Horizon 2020 research and innovation programme under the Marie Skłodowska-Curie Grant Agreement No. 841556. O.B. and I.D.S. also acknowledge support by the Federal Ministry of Education and Research (BMBF, Germany) project number 033RC021B within the CO_2-WIN initiative. The authors thank Stefan Oswald for support with the XPS system.

Open access funding enabled and organized by Projekt DEAL.

Conflict of Interest

The authors declare no conflict of interest.

Author Contributions

A.H. and J.D.B contributed equally to this work. All authors have given approval to the final version of the manuscript.

Data Availability Statement

The data that support the findings of this study are available from the corresponding author upon reasonable request.

Keywords

aluminum oxide monolayers, atomic layer deposition, gallium nitride, interface engineering, self-assembled monolayers, X-ray photoelectron spectroscopy

Received: February 9, 2021
Revised: April 13, 2021
Published online:

© 2021 The Authors. Advanced Functional Materials published by Wiley-VCH GmbH

[1] R. W. Johnson, A. Hultqvist, S. F. Bent, *Mater. Today* **2014**, *17*, 236.
[2] a) X. Yang, E. Aydin, H. Xu, J. Kang, M. Hedhili, W. Liu, Y. Wan, J. Peng, C. Samundsett, A. Cuevas, S. De Wolf, *Adv. Energy Mater.* **2018**, *8*, 1800608; b) X. Yang, K. Weber, Z. Hameiri, S. De Wolf, *Prog. Photovoltaics* **2017**, *25*, 896.
[3] A. G. Scheuermann, P. C. McIntyre, *J. Phys. Chem. Lett.* **2016**, *7*, 2867.
[4] a) C. Marichy, M. Bechelany, N. Pinna, *Adv. Mater.* **2012**, *24*, 1017; b) P. Varadhan, H.-C. Fu, D. Priante, J. R. D. Retamal, C. Zhao, M. Ebaid, T. K. Ng, I. Ajia, S. Mitra, I. S. Roqan, B. S. Ooi, J.-H. He, *Nano Lett.* **2017**, *17*, 1520.
[5] S. M. George, *Chem. Rev.* **2010**, *110*, 111.
[6] P. Laukkanen, M. P. J. Punkkinen, M. Kuzmin, K. Kokko, J. Lång, R. M. Wallace, *Appl. Phys. Rev.* **2021**, *8*, 011309.
[7] E. A. Jones, F. F. Wang, D. Costinett, *IEEE Trans. Emerg. Sel. Topics Power Electron.* **2016**, *4*, 707.
[8] a) X. Wu, R. Liang, L. Guo, L. Liu, L. Xiao, S. Shen, J. Xu, J. Wang, *Appl. Phys. Lett.* **2016**, *109*, 232101; b) B. S. Eller, J. Yang, R. J. Nemanich, *J. Vac. Sci. Technol., A* **2013**, *31*, 050807; c) J. Son, V. Chobpattana, B. M. McSkimming, S. Stemmer, *J. Vac. Sci. Technol., A* **2015**, *33*, 020602; d) Y. Jia, K. Zeng, U. Singisetti, *J. Appl. Phys.* **2017**, *122*, 154104.
[9] M. Aykol, K. A. Persson, *ACS Appl. Mater. Interfaces* **2018**, *10*, 3039.
[10] P. H. Lewis, R. Rundle, *J. Chem. Phys.* **1953**, *21*, 986.
[11] S. E. Potts, H. B. Profijt, R. Roelofs, W. M. Kessels, *Chem. Vap. Deposition* **2013**, *19*, 125.
[12] a) M. M. Frank, G. D. Wilk, D. Starodub, T. Gustafsson, E. Garfunkel, Y. J. Chabal, J. Grazul, D. A. Muller, *Appl. Phys. Lett.* **2005**, *86*, 152904; b) M. L. Huang, Y. C. Chang, C. H. Chang, Y. J. Lee, P. Chang, J. Kwo, T. B. Wu, M. Hong, *Appl. Phys. Lett.* **2005**, *87*, 252104; c) C. L. Hinkle, A. M. Sonnet, E. M. Vogel, S. McDonnell, G. J. Hughes, M. Milojevic, B. Lee, F. S. Aguirre-Tostado, K. J. Choi, H. C. Kim, J. Kim, R. M. Wallace, *Appl. Phys. Lett.* **2008**, *92*, 071901; d) M. Milojevic, F. S. Aguirre-Tostado, C. L. Hinkle, H. C. Kim, E. M. Vogel, J. Kim, R. M. Wallace, *Appl. Phys. Lett.* **2008**, *93*, 202902; e) B. Brennan, H. Dong, D. Zhernokletov, J. Kim, R. M. Wallace, *Appl. Phys. Express* **2011**, *4*, 125701; f) H. Dong, B. Brennan, X. Qin, D. M. Zhernokletov, C. L. Hinkle, J. Kim, R. M. Wallace, *Appl. Phys. Lett.* **2013**, *103*, 121604.
[13] a) A. D. Carter, W. J. Mitchell, B. J. Thibeault, J. J. M. Law, M. J. W. Rodwell, *Appl. Phys. Express* **2011**, *4*, 091102; b) L. B. Ruppalt, E. R. Cleveland, J. G. Champlain, S. M. Prokes, J. B. Boos, D. Park, B. R. Bennett, *Appl. Phys. Lett.* **2012**, *101*, 231601; c) S. Gu, E. A. Chagarov, J. Min, S. Madisetti, S. Novak, S. Oktyabrsky, A. J. Kerr, T. Kaufman-Osborn, A. C. Kummel, P. M. Asbeck, *Appl. Surf. Sci.* **2014**, *317*, 1022.
[14] a) R. L. Puurunen, *J. Appl. Phys.* **2005**, *97*, 121301; b) R. L. Puurunen, W. Vandervorst, *J. Appl. Phys.* **2004**, *96*, 7686.
[15] R. L. Puurunen, *Chem. Vap. Deposition* **2003**, *9*, 327.
[16] G. N. Parsons, *J. Vac. Sci. Technol., A* **2019**, *37*, 020911.
[17] Y. Irokawa, T. T. Suzuki, K. Yuge, A. Ohi, T. Nabatame, K. Kimoto, T. Ohnishi, K. Mitsuishi, Y. Koide, *Jpn. J. Appl. Phys.* **2017**, *56*, 128004.
[18] S. Klejna, S. D. Elliott, *Chem. Mater.* **2014**, *26*, 2427.
[19] M. Avrami, *J. Chem. Phys.* **1940**, *8*, 212.
[20] a) C. Barbos, D. Blanc-Pelissier, A. Fave, C. Botella, P. Regreny, G. Grenet, E. Blanquet, A. Crisci, M. Lemiti, *Thin Solid Films* **2016**, *617*, 108; b) A. W. Ott, K. C. McCarley, J. W. Klaus, J. D. Way, S. M. George, *Appl. Surf. Sci.* **1996**, *107*, 128.
[21] R. L. Puurunen, *Chem. Vap. Deposition* **2003**, *9*, 249.
[22] Y. J. Lee, S.-W. Kang, *Electrochem. Solid-State Lett.* **2002**, *5*, C91.
[23] O. M. E. Ylivaara, X. Liu, L. Kilpi, J. Lyytinen, D. Schneider, M. Laitinen, J. Julin, S. Ali, S. Sintonen, M. Berdova, E. Haimi, T. Sajavaara, H. Ronkainen, H. Lipsanen, J. Koskinen, S.-P. Hannula, R. L. Puurunen, *Thin Solid Films* **2014**, *552*, 124.
[24] a) T. Maruyama, Y. Miyajima, S. H. Cho, K. Akimoto, H. Kato, *Physica B* **1999**, *262*, 240; b) N. J. Shevchik, J. Tejeda, M. Cardona, *Phys. Rev. B* **1974**, *9*, 2627.
[25] K. Prabhakaran, T. G. Andersson, K. Nozawa, *Appl. Phys. Lett.* **1996**, *69*, 3212.
[26] X. Qin, H. Dong, B. Brennan, A. Azacatl, J. Kim, R. M. Wallace, *Appl. Phys. Lett.* **2013**, *103*, 221604.
[27] a) P. Sivasubramani, T. J. Park, B. E. Coss, A. Lucero, J. Huang, B. Brennan, Y. Cao, D. Jena, H. Xing, R. M. Wallace, J. Kim, *Phys. Status Solidi RRL* **2012**, *6*, 22; b) Y. Jia, J. S. Wallace, E. Echeverria, J. A. GardellaJr., U. Singisetti, *Phys. Status Solidi B* **2017**, *254*, 1600681.
[28] B. Brennan, X. Qin, H. Dong, J. Kim, R. M. Wallace, *Appl. Phys. Lett.* **2012**, *101*, 211604.
[29] J. A. Rotole, P. M. A. Sherwood, *Surf. Sci. Spectra* **1998**, *5*, 11.
[30] S. A. Paniagua, A. J. Giordano, O. N. L. Smith, S. Barlow, H. Li, N. R. Armstrong, J. E. Pemberton, J.-L. Brédas, D. Ginger, S. R. Marder, *Chem. Rev.* **2016**, *116*, 7117.
[31] H. Kim, P. E. Colavita, P. Paoprasert, P. Gopalan, T. F. Kuech, R. J. Hamers, *Surf. Sci.* **2008**, *602*, 2382.
[32] E. L. Hanson, J. Schwartz, B. Nickel, N. Koch, M. F. Danisman, *J. Am. Chem. Soc.* **2003**, *125*, 16074.
[33] M. J. Pellerite, T. D. Dunbar, L. D. Boardman, E. J. Wood, *J. Phys. Chem. B* **2003**, *107*, 11726.
[34] M. Dubey, T. Weidner, L. J. Gamble, D. G. Castner, *Langmuir* **2010**, *26*, 14747.
[35] R. Zhao, P. Rupper, S. Gaan, *Coatings* **2017**, *7*, 133.
[36] B. L. Pearce, S. J. Wilkins, T. Paskova, A. Ivanisevic, *J. Mater. Res.* **2015**, *30*, 2859.
[37] M. Textor, L. Ruiz, R. Hofer, A. Rossi, K. Feldman, G. Hähner, N. D. Spencer, *Langmuir* **2000**, *16*, 3257.
[38] M. Wagstaffe, A. G. Thomas, M. J. Jackman, M. Torres-Molina, K. L. Syres, K. Handrup, *J. Phys. Chem. C* **2016**, *120*, 1693.
[39] C. Schuschke, M. Schwarz, C. Hohner, T. N. Silva, L. Fromm, T. Döpper, A. Görling, J. Libuda, *J. Phys. Chem. Lett.* **2018**, *9*, 1937.
[40] R. Luschtinetz, A. F. Oliveira, H. A. Duarte, G. Seifert, *Z. Anorg. Allg. Chem.* **2010**, *636*, 1506.
[41] S. C. D'Andre, A. Y. Fadeev, *Langmuir* **2003**, *19*, 7904.
[42] R. T. Sanderson, *J. Chem. Educ.* **1988**, *65*, 112.
[43] a) J. Yang, B. S. Eller, R. J. Nemanich, *J. Appl. Phys.* **2014**, *116*, 123702; b) J. H. Dycus, K. J. Mirrielees, E. D. Grimley, R. Kirste, S. Mita, Z. Sitar, R. Collazo, D. L. Irving, J. M. LeBeau, *ACS Appl. Mater. Interfaces* **2018**, *10*, 10607.
[44] D.-w. Choi, K.-B. Chung, J.-S. Park, *Thin Solid Films* **2013**, *546*, 31.
[45] K. Henkel, M. Kot, D. Schmeißer, *J. Vac. Sci. Technol., A* **2017**, *35*, 01B125.
[46] O. A. Dicks, J. Cottom, A. L. Shluger, V. V. Afanas'ev, *Nanotechnology* **2019**, *30*, 205201.
[47] S. Ganguly, J. Verma, G. Li, T. Zimmermann, H. Xing, D. Jena, *Appl. Phys. Lett.* **2011**, *99*, 193504.
[48] a) T.-H. Hung, K. Sasaki, A. Kuramata, D. N. Nath, P. S. Park, C. Polchinski, S. Rajan, *Appl. Phys. Lett.* **2014**, *104*, 162106; b) M. Esposto, S. Krishnamoorthy, D. N. Nath, S. Bajaj, T.-H. Hung, S. Rajan, *Appl. Phys. Lett.* **2011**, *99*, 133503.
[49] D. M. Taylor, O. N. De Oliveira, H. Morgan, *J. Colloid Interface Sci.* **1990**, *139*, 508.
[50] S. Jang, D. Son, S. Hwang, M. Kang, S.-K. Lee, D.-Y. Jeon, S. Bae, S. H. Lee, D. S. Lee, T.-W. Kim, *Nano Convergence* **2018**, *5*, 20.
[51] J. Kirschner, Z. Wang, S. Eigler, H.-P. Steinrück, C. M. Jäger, T. Clark, A. Hirsch, M. Halik, *Nanoscale* **2014**, *6*, 11344.
[52] J. B. Rivest, G. Li, I. D. Sharp, J. B. Neaton, D. J. Milliron, *J. Phys. Chem. Lett.* **2014**, *5*, 2450.
[53] Y. Dong, R. M. Feenstra, J. E. Northrup, *J. Vac. Sci. Technol., B* **2006**, *24*, 2080.
[54] X. Qin, H. Dong, J. Kim, R. M. Wallace, *Appl. Phys. Lett.* **2014**, *105*, 141604.

© 2021 The Authors. Advanced Functional Materials published by Wiley-VCH GmbH

[55] K. Lee, S. Donovan, B. Gila, M. Overberg, J. Mackenzie, C. Abernathy, R. Wilson, *J. Electrochem. Soc.* **2000**, *147*, 3087.
[56] a) T. Hashizume, S. Ootomo, T. Inagaki, H. Hasegawa, *J. Vac. Sci. Technol., B* **2003**, *21*, 1828; b) M. F. Romero, A. Jiménez, J. Miguel-Sánchez, A. F. Braña, F. González-Posada, R. Cuerdo, F. Calle, E. Muñoz, *IEEE Electron Device Lett.* **2008**, *29*, 209.
[57] L. Lymperakis, J. Neugebauer, M. Himmerlich, S. Krischok, M. Rink, J. Kröger, V. M. Polyakov, *Phys. Rev. B* **2017**, *95*, 195314.
[58] A. J. Kerr, E. Chagarov, S. Gu, T. Kaufman-Osborn, S. Madisetti, J. Wu, P. M. Asbeck, S. Oktyabrsky, A. C. Kummel, *J. Chem. Phys.* **2014**, *141*, 104702.

 © 2021 The Authors. Advanced Functional Materials published by Wiley-VCH GmbH